When subcellular chemical imaging enlightens our understanding on intestinal absorption, intracellular fate and toxicity of PFOA in vitro

Charlotte B.A. Stoffels, Sébastien Cambier, Maria Subirana, Dirk Schaumlöffel, Gemma Gomez, Denis Pittois, Cédric Guignard, Jens Schwamborn, Tom Wirtz, Arno Gutleb, et al.

Journal of Hazardous Materials 480 (2024) 136205

Contents lists available at ScienceDirect

Journal of Hazardous Materials

journal homepage: www.elsevier.com/locate/jhazmat

When subcellular chemical imaging enlightens our understanding on intestinal absorption, intracellular fate and toxicity of PFOA in vitro

Charlotte B.A. Stoffels [a,b,c,*], Sébastien Cambier [b], Maria A. Subirana [d], Dirk Schaumlöffel [d], Gemma Gomez [e], Denis Pittois [b], Cédric Guignard [b], Jens C. Schwamborn [e], Tom Wirtz [a], Arno C. Gutleb [b], Muriel Mercier-Bonin [f], Jean-Nicolas Audinot [a]

[a] Materials Research and Technology (MRT) Department, Luxembourg Institute of Science and Technology, Belvaux, Luxembourg
[b] Environmental Research and Innovation (ERIN) Department, Luxembourg Institute of Science and Technology, Belvaux, Luxembourg
[c] Faculty of Science, Technology and Medicine, University of Luxembourg, Esch-sur-Alzette, Luxembourg
[d] CNRS, Université de Pau et des Pays de l'Adour, E2S UPPA, Institut des Sciences Analytiques et de Physico-Chimie pour l'Environnement et les Matériaux (IPREM), UMR 5254 Pau, France
[e] Luxembourg Centre for Systems Biomedicine, University of Luxembourg, Esch-sur-Alzette, Luxembourg
[f] Toxalim, Université de Toulouse, INRAE, INP-ENVT, INP-EI-Purpan, Université de Toulouse 3 Paul Sabatier, Toulouse, France

HIGHLIGHTS

- High-resolution analytical imaging enables PFAS localization at subcellular level.
- Intracellular PFAS concentrations can be estimated by high-resolution analytical imaging.
- PFOA highly increases the metabolic activity of intestinal cells at low doses.
- PFOA mainly accumulates in the cytosol of intestinal cells.

GRAPHICAL ABSTRACT

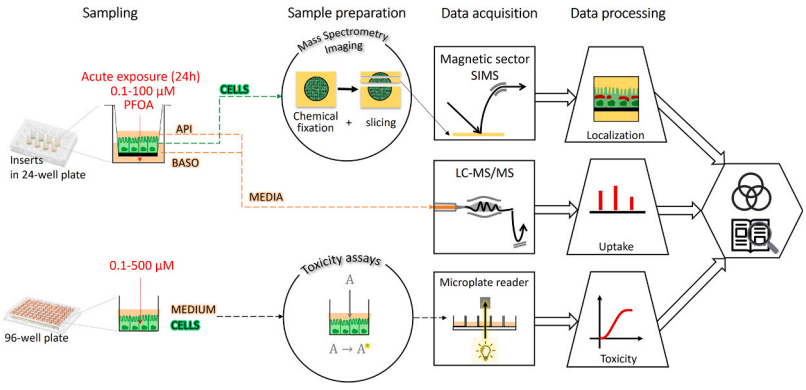

ARTICLE INFO

Keywords:
PFAS
SIMS
Imaging
In vitro toxicology
Intestinal model

ABSTRACT

Perfluorooctanoic acid (PFOA) is a persistent organic pollutant that accumulates in the human body, leading to major health issues. Upon oral uptake, the gastrointestinal tract is the first biological barrier against PFOA. However, the localization of PFOA and its impact on the intestinal wall are largely unknown. Here we achieve a breakthrough in the knowledge of intestinal absorption, intracellular fate and toxicity of PFOA using in vitro assays combined with novel analytical imaging techniques. For the first time, we localized PFOA in the cytosol of Caco-2 cells after acute exposure using high spatial resolution mass spectrometry imaging, and we estimated the PFOA cytosolic concentration. Knowing that PFOA enters and accumulates in the intestinal cells, we also performed common toxicity assays assessing cell metabolic activity, membrane integrity, oxidative stress response, and cell respiration. This study integrating powerful analytical techniques with widely used toxicology assays

* Corresponding author at: Materials Research and Technology (MRT) Department, Luxembourg Institute of Science and Technology, Belvaux, Luxembourg.
E-mail address: charlotte.stoffels@list.lu (C.B.A. Stoffels).

https://doi.org/10.1016/j.jhazmat.2024.136205
Received 6 February 2024; Received in revised form 7 October 2024; Accepted 16 October 2024
Available online 18 October 2024

provides insightful information to better understand potential negative impacts of PFOA and opens new opportunities in toxicology and life science in general.

1. Introduction

Per- and polyfluoroalkylated substances (PFAS), such as perfluorooctanoic acid (PFOA), have been widely used for many industrial purposes and consumer-related applications, such as cookware, carpets, clothes or packaging, and are therefore omnipresent in our environment [1]. However, these chemicals are persistent and accumulate in the human body, leading to major health issues. Health impact of PFAS is currently a very hot topic as illustrated in the literature and will continue to be for a long time.

Among all exposure pathways, dietary intake and drinking water have been identified as two principal routes of human exposure [2]. Upon oral exposure, PFAS are highly absorbed by the intestine [3] entering the bloodstream and conveying to various tissues, but PFAS can also accumulate directly in the intestinal barrier [4]. PFAS accumulation could cause damage of that barrier, leading to an increase in epithelium permeability, tight junction disruption, protective mucus layer reduction, gut microbiota imbalance, inflammation, to name but a few [5,6]. Although the gastrointestinal tract is the first biological barrier against these ingested perfluorinated compounds, little is known about the health impacts of PFAS, including PFOA, on the intestine.

Among others, it has been reported that the development of ulcerative colitis (an intestinal bowel disease (IBD) characterized by a defective intestinal barrier) was significantly associated with PFOA exposure in humans [7]. In mice, it has been reported that PFOA highly bioaccumulates in the small intestine and colon. Stronger effects were found in the small intestine due to an increased accumulation of PFOA [8]. Another study indicates that PFOA exposure impairs intestinal barrier integrity and causes gut inflammation [5]. Exposure to perfluorooctane sulfonic acid (PFOS) has also been found to alter the gut microbiome [9]. Although in vitro studies are widely used in hazard assessment, few of them have evaluated the toxic effects of PFOA on human intestinal cells. PFOA has been observed to alter calcium homeostasis and decrease colon carcinoma (HCT116) cell viability over time [10,11]. Another study confirmed that PFOA could induce an increased invasiveness of colorectal cancer cells (DLD-1 cells), suggesting the role of PFOA in cancer metastasis [12]. Regarding intestinal absorption, PFOA appears to be taken up from the apical membrane of human intestinal Caco-2 cells via a passive diffusion and transport-mediated process (at least in part by organic anion transporting polypeptides (OATP)) [13].

Overall, the fate of PFAS after exposure, and especially their localization at subcellular level, have rarely been studied, especially due to the lack of adequate physicochemical methods. The distribution of PFOA in subcellular fractions was previously evaluated in rat liver and kidney by liquid scintillation counting [14], which requires the use of radio isotopes ([1-^{14}C]PFOA). Moreover, an important limitation of the current in vitro studies on PFAS remains the lack of information on intracellular concentration, which would allow better comparison with real exposures and support toxic effects. The PFOA intracellular concentration was previously evaluated in Caco-2 cells using gas chromatography mass spectrometry (GC-MS) [13]. One main disadvantage of such technique is the extraction step, inevitably understating the real value. Therefore, performing in vitro studies including the localization at subcellular level and ideally the direct quantification in the regions of interest (ROIs) would definitely push forward toxicology studies on PFAS.

In the present study, we have developed a workflow based on complementary multi-technical approach, combining high spatial resolution mass spectrometry imaging techniques (i.e., magnetic sector secondary ion mass spectrometry, abbrev. magnetic sector SIMS) allowing the localization and semi-quantification of PFOA inside the cells, bulk analytical technique (i.e., liquid chromatography with tandem mass spectrometry, abbrev. LC-MS/MS) enabling the quantification of PFOA inside the cell media (i.e., apical and basolateral media), and common cell toxicity assays (i.e., tests on cell metabolic activity, membrane integrity, oxidative stress response, and cell respiration). More precisely, the subcellular imaging was carried out using the NanoSIMS instrument for the isotopic measurement with high accuracy [15,16], and the state-of-the-art focused ion beam scanning electron microscope (FIB--SEM) coupled with an in-house-designed magnetic sector SIMS (FIB--SEM-SIMS) for in situ correlative microscopy at sub-15 nm SIMS spatial resolution [17,18]. The Caco-2 cell monolayer was selected as our in vitro model because of its morphological and functional similarity to human small intestinal epithelial cells [19]. This workflow reveals the intestinal absorption, intracellular fate and concentration of PFOA considering Caco-2 cells and the mechanisms of toxicity, and could be extended to other perfluorinated compounds or in vitro cell models. This study paves the way for further toxicology research, integrating powerful analytical techniques with widely used toxicology assays.

2. Results

2.1. PFOA intracellular localization

After 24-h exposure, PFOA was successfully localized inside the Caco-2 cells grown on insert for all exposure concentrations [0.1–100 μM] using the FIB-SEM-SIMS instrument (Fig. 1A-H). PFOA was localized by tracking the fluoride ($^{19}F^-$, red) while the cell structure was identified using carbon-nitrogen molecular ions ($^{12}C^{14}N^-$, green). As the PFOA distribution was similar for all exposure concentrations, only one image (5 μM) is further described hereafter (Fig. 2). Thanks to FIB-SEM-SIMS capabilities, the SIMS images of $^{19}F^-$ (Fig. 2A) and $^{12}C^{14}N^-$ (Fig. 2B) were further correlated with back-scattered electron (BSE) image (Fig. 2C) within the same instrument. Using adequate post-staining agent such as osmium tetroxide, BSE images revealed the cell structure and the localization of lipid droplets [20], based on the average atomic number of atoms (Fig. 2C). The image overlay confirmed the uptake of PFOA by the cells and unveiled its localization inside the cells (Fig. 2D). Indeed, PFOA was mainly localized in the cell cytosol, and was not detected in the protein-rich structures like the nucleus or the cell membrane (Fig. 2D, green) or in the lipid droplets (Fig. 2D, yellow). Its main localization inside the cytosol was further confirmed using the NanoSIMS instrument (Fig. 3A). The better sensitivity of NanoSIMS related to the use of Cs^+ primary ions (but poorer spatial resolution and lower analysis throughput than FIB-SEM-SIMS) allowed to also detect $^{19}F^-$ in the cell membrane (Fig. 3B1), at the interface between the cell and the insert, at the junction between two cells (Fig. 3B2), but at a lesser extent. However, as observed by FIB-SEM-SIMS, no PFOA was detected in the nucleus (Fig. 3A, green).

2.2. PFOA quantification in the cytosol

The PFOA quantification in the cytosol was assessed based on FIB-SEM-SIMS images in Fig. 1. While increasing the PFOA exposure concentration (from 0.1 to 100 μM), the PFOA signal in the cytosol followed a logarithmic profile (Fig. 4A). The cytosolic PFOA concentration starts to saturate at around 1 μM PFOA exposure concentration. The $^{19}F^-$ signal in the cytosol was normalized by the $^{12}C_2^-$ signal, and the ratio was further converted to concentration using a calibration curve (see experimental section). The cytosolic PFOA concentration reached a maximum of approximately 6 mM for a nominal exposure concentration

of 50 μM (Fig. 4B), which is then 120 times higher than the latter.

The results for low PFOA exposure concentrations (from 0.5 to 5 μM) were further confirmed by NanoSIMS using 8-fold ^{13}C labelling of the PFOA molecule. Indeed, Fig. 5 shows the same trend as observed in Fig. 4, with a threshold already achieved at 1 μM. For NanoSIMS analysis, concentrations higher than 5 μM were not tested because $^{13}C_8$-PFOA was received diluted in 100 % methanol and higher concentrations (> 5 % methanol) would have been cytotoxic for the cells.

2.3. PFOA quantification in the cell media

PFOA was quantified in the apical (API) and basolateral (BASO) media for the different exposure concentrations using LC-MS/MS technique. The quantity of PFOA in the API (orange) and BASO (blue) increased linearly with exposure concentration; however, the slope for BASO was significantly smaller (Fig. 6). Based on both the initial quantity of PFOA and the measured quantity in the API and BASO media after exposure, the quantity inside the cells was calculated (yellow). The calculation was performed as follows:

$$n_{API,i} = n_{CELL,f} + n_{BASO,f} + n_{API,f}$$

$$n_{CELL,f} = n_{API,i} - n_{API,f} - n_{BASO,f}$$

Where:

- $n_{API,i}$ is the initial quantity added in the apical compartment (exposure dose),
- $n_{API,f}$ is the final quantity (after 24 h) in the apical compartment,
- $n_{BASO,f}$ is the final quantity in the basolateral compartment, and
- $n_{CELL,f}$ is the final quantity in the cells.

Of note, this quantity does not take into account the potential interactions of PFOA with the well/insert and may therefore be overestimated. The curve shows a rapid accumulation in the cells when the quantity in the BASO was still zero, and then a plateau when PFOA was released in the BASO medium above 25 μM.

Even if the quantification from FIB-SEM-SIMS images (Fig. 4) and LC-MS/MS (Fig. 6, yellow) show similar trends (saturation curves), they cannot directly be compared. Indeed, the first quantification only focuses on the cytosolic compartment and gives an approximate concentration in this compartment, while the second one focuses on the entire cells and gives an approximate quantity (nmol). However, if we assume that all PFOA only accumulates in the cell cytosol, we can use the following equation:

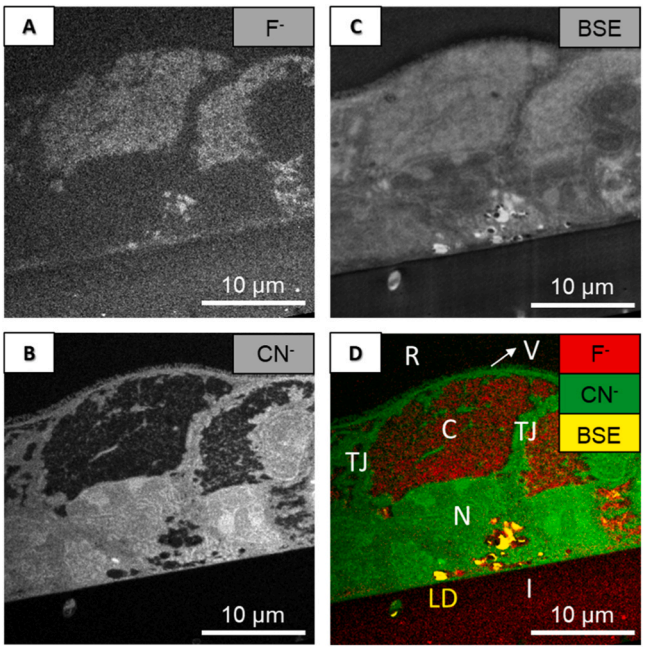

Fig. 2. Localization of PFOA inside Caco-2 cells by FIB-SEM-SIMS. (**A**) $^{19}F^-$ image provides the localization of PFOA. (**B**) $^{12}C^{14}N^-$ image gives the structure of the cells. (**C**) BSE image indicates the cell structure and the localization of lipid droplets. (**D**) The overlay of SIMS (**A, B**) and BSE (**C**) images allows the localization of PFOA (red) and the lipid droplets (yellow) inside the cells (green). The threshold intensity of the BSE images was adjusted to highlight only the brighter cellular components, namely lipid droplets, the latter of which were stained yellow to sharpen the images. The letters correspond to C = cytoplasm, I = insert, LD = lipid droplets, N = nucleus, R = resin, T*J* = tight junction and V = microvilli.

$$n_{PFOA,total} = C_{PFOA,cytosol} \times N_{cells} \times V_{cytosol} \quad (1)$$

where $n_{PFOA,total}$ is the total number of moles of PFOA in the cell monolayer, $C_{PFOA,cytosol}$ is the concentration of PFOA in the cell cytosol (calculated using SIMS images), N_{cells} is the number of cells on the insert, $V_{cytosol}$ is the cytosolic volume.

By applying this formula, the PFOA concentrations from Fig. 4 ($C_{PFOA,cytosol}$) can be converted to total PFOA quantities ($n_{PFOA,total}$) as for

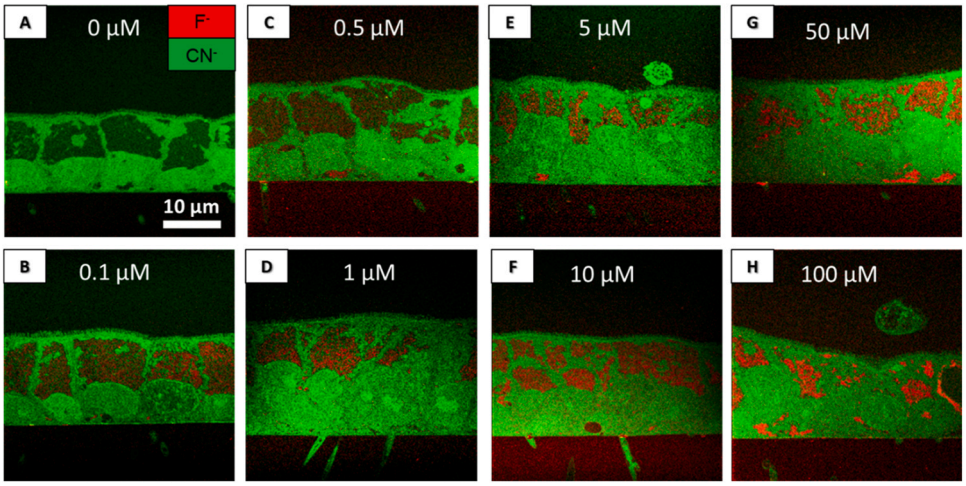

Fig. 1. PFOA localization and signal intensity inside the Caco-2 cells for different exposure concentrations using FIB-SEM-SIMS instrument. PFOA is identified by the signal of $^{19}F^-$ (red) and cell morphology can be observed using the $^{12}C^{14}N^-$ signal (green). (**A-H**) correspond to 0–100 μM. One representative image per concentration is given.

LC-MS/MS results (Fig. 7). The parameters were estimated as follows: N_{cells} = 1E+ 06 cells/insert and $V_{cytosol}$ = 2.08 pL/cell for Caco-2 cells (averaging from the literature [21]). The saturation curve reaches a plateau of 12 nmol, which is the same order of magnitude as the value calculated with LC-MS/MS (6 nmol, Fig. 6A). Both techniques showed quite similar results with slight variations due to the assumptions made.

Knowing now that PFOA is entering and accumulating in the cytosol Caco-2 cells, and that many metabolic pathways occurs in the cytosol, a series of assays were performed to assess its metabolic and toxicological impact on the cells.

2.4. Cellular metabolic activity and viability

The metabolic activity after exposure to PFOA was assessed using resazurin and ATP assays. Those assays are usually used to assess cell proliferation; however, they may not accurately reflect cell proliferation rates due to a miscorrelation between metabolic activity and cell number [22–24]. Indeed, we also performed a cell proliferation assay quantifying cellular DNA content (CyQUANT), which did not show any impact of PFOA on the cell number (data not shown). On the contrary, the resazurin assay has revealed a high impact of PFOA on the cell metabolic activity (Fig. 8A). It is increasing at low dose until reaching a maximum (120 %) at 1–10 μM, then decreasing and returning to the control value (100 %) at 500 μM. We also performed an ATP assay, in order to know if this high metabolic activity under PFOA exposure was also visible at the level of the cellular energetic resources that mainly related to the cellular ATP level. Even though a similar trend was observed (except for 500 μM), the ATP levels measured in the exposed cells were not significantly different from the control (Fig. 8C).

2.5. Cell membrane integrity

The potential disruption of membrane integrity after PFOA exposure was assessed by measuring the release of lactate dehydrogenase (LDH). The overall trend over the concentration range showed a decrease in the release of LDH, reaching a minimum at 0.5–1 μM PFOA, and then an increase until reaching a plateau similar to the control (Fig. 8B). It is worth noting that the results constitute a mirror image when compared to the resazurin assay. This indicates that the cells at low-dose PFOA exposure are metabolically more active and release less LDH.

2.6. Cell oxidative stress response

Reactive oxygen species (ROS) generation after PFOA exposure was quantified using DCFH-DA assay, measuring the overall cell oxidative stress. Only the PFOA exposure at 500 μM significantly increased the generation of ROS (Fig. 8D), yet such exposure concentration is undoubtedly not realistic.

2.7. Cell respiration

The cell respiration after PFOA exposure was assessed using the Seahorse assay. The Seahorse analyzer measures the oxygen consumption rate (OCR), an indicator of mitochondrial respiration, of the living Caco-2 cells previously exposed to PFOA. It provides information on different parts of the mitochondrial respiration, which are detailed in the supplementary materials.

We observed almost no effect on the mitochondrial respiration (Fig. 8E-H). The maximal respiration (Fig. 8E) and the spare capacity (Fig. 8F) were the only parameters changing according to PFOA exposure concentration. The maximal respiration and the SPR followed the same trend: the OCRs were decreasing for the lowest concentration (0.1 μM), then increasing for higher concentrations until reaching a plateau (except at 500 μM for which OCRs decreased again). The difference with the control was only significant for one concentration (50 μM), characterized by a higher maximal respiration and SPR, which means a higher capacity to meet additional energy demands. It is worth noting that the ATP production (Fig. 8G) follows a very similar trend to the ATP assay results (Fig. 8C), which further confirms our findings.

3. Discussion

The fate of PFAS following oral exposure, particularly their localization at the subcellular level, has received less attention, notably owing to a lack of appropriate physicochemical techniques. Furthermore, one of the major limitations of existing PFAS in vitro studies is the lack of information on intracellular concentration, which would allow for better comparison with real exposures and association with harmful effects. As a result, in vitro testing involving subcellular localization and, ideally, direct concentration measurement in the regions of interest (ROIs) will undoubtedly advance PFAS toxicity research.

In this study, we have focused on PFOA, as a major representative of PFAS, and developed a complementary multi-technical approach, revealing its intestinal absorption, intracellular fate and concentration, and also toxicity considering Caco-2 cells, but which could be applied to additional perfluorinated chemicals or cell culture models. For that purpose, we have combined (i) cutting-edge high-resolution chemical imaging techniques (i.e., FIB-SEM-SIMS and NanoSIMS) allowing localization and semi-quantification of PFOA inside the cells, (ii) a bulk analytical technique (i.e., LC-MS/MS) enabling the separation, identification, and quantification of PFOA inside the cell media (i.e., apical and basolateral media), and (iii) common cell toxicity assays.

FIB-SEM-SIMS analysis confirmed the uptake of PFOA by the intestinal cells for all exposure concentrations [0.1–100 μM] (Fig. 1) and showed that it accumulates mainly in the membrane-free cell cytosol (Fig. 2), which was further confirmed by NanoSIMS on limited ROIs (Fig. 3). This confirms previous studies demonstrating the high proportion of PFOA inside the membrane-free cytosol of cells present in rat

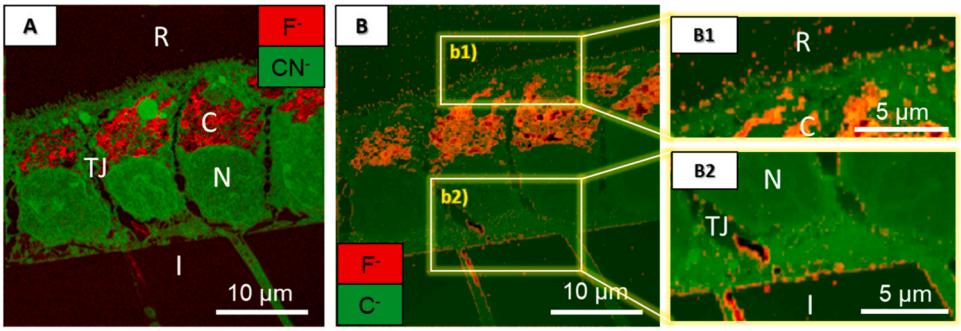

Fig. 3. Localization of PFOA inside Caco-2 cells by NanoSIMS. (**A**) $^{19}F^-$ image provides the localization of PFOA and $^{12}C^{14}N^-$image indicates the structure of the cells. (**B**) PFOA localization at the resin-cell interface (**B1**), at the cell-cell and the cell-insert interfaces (**B2**). The letters correspond to C = cytosol, I = insert, N = nucleus, R = resin, T*J* = tight junction.

kidney and liver [14]. Therefore, we can assume that PFOA would mainly interact with the cytosolic part of the cells, and potentially impair some metabolic pathways, such as signal transduction between the cell membrane and the nucleus and organelles, metabolite transport activities, cell division, and energetic metabolism [25]. Moreover, NanoSIMS analysis also enabled the PFOA localization in the cell membrane, at the interface between the cell and the insert, and at the junction between two adjacent cells, but at a lesser extent than in the cytosol. Although the amount of PFOA in other parts of the cell was lower, it could still impact other key cell functions. As confirmed by Fig. 2, PFOA does not accumulate in lipid droplets. Unlike hydrocarbon chains that are hydrophobic and lipophilic, the perfluorinated chains of PFAS are both hydrophobic and lipophobic. However, the functional group (e.g., a charged moiety such as a carboxylic group for PFOA) gives a slight hydrophilicity to a part of the molecule. Furthermore, fluorine is a highly electronegative element, which imparts polarity and makes PFAS polar chemicals [26]. Therefore, the physico-chemical properties of PFOA, coupled with the cytosol's high-water content of approximately 70 % by volume [27], likely contribute to its predominant accumulation in the cytosol. Additionally, PFOA is known to distribute throughout the body bound to proteins such as human serum albumin [28]. Given that the cytosol is also rich in proteins (comprising 20–30 % by volume) [27], it is plausible that a portion of PFOA binds to cytosolic proteins. Moreover, structurally resembling fatty acids, PFAS including PFOA may engage in similar interactions and compete with cytosolic fatty acids for binding sites and metabolic pathways [29].

The PFOA concentration in the cell cytosol was assessed based on FIB-SEM-SIMS images (Fig. 4). It appears that the intracellular concentration followed a logarithmic profile while increasing the exposure concentration, until reaching a threshold at around 1 μM (Fig. 4), which was also confirmed by NanoSIMS using ^{13}C labelling of the PFOA molecule (Fig. 5). The plateau concentration was two orders of magnitude higher than the nominal exposure concentration, confirming the high accumulation of PFOA in intestinal cells. As the relationship between the initial PFOA concentration and its final intracellular concentration is saturable, it suggests a transport-mediated process, corroborating previous studies [13].

PFOA was also quantified in the cell media by LC-MS/MS analysis (Fig. 6). In both compartments (apical and basolateral media), the quantity increased linearly with exposure concentration; however, the increase was less pronounced in the basolateral medium. From those results, the quantity inside the cells was estimated. Besides, based on some assumptions, the cytosolic PFOA concentration determined by FIB-SEM-SIMS was converted to total PFOA quantities (Fig. 7), which could therefore be compared to quantities estimated by LC-MS/MS. Both analyses showed a logarithmic curve while increasing the exposure concentration, until reaching a plateau of 12 nmol and 6 nmol by FIB-SEM-SIMS and LC-MS/MS, respectively, which provides quite similar results given the assumptions made.

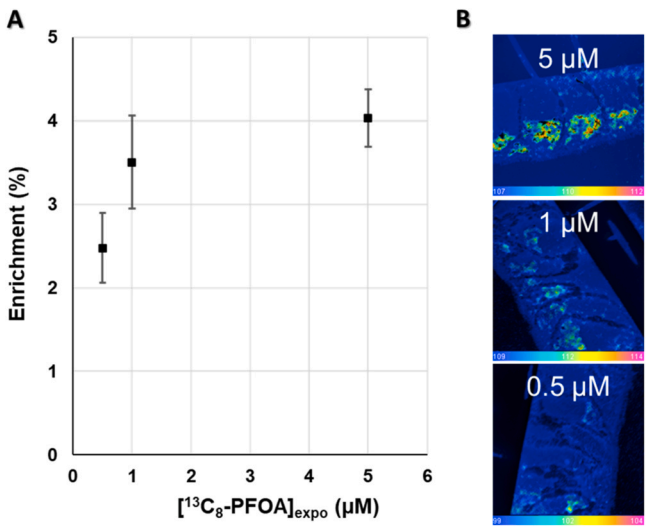

Fig. 5. Intracellular distribution and concentration of $^{13}C_8$-PFOA by NanoSIMS. (**A**) Enrichment (calculated as ($[^{13}C/^{12}C]_{cytosol} - [^{13}C/^{12}C]_{natural}$)/$[^{13}C/^{12}C]_{natural}$* 100) in function of the PFOA exposure concentration. (**B**) Intracellular distribution and enrichment in $^{13}C_8$-PFOA for different exposure concentrations (0.5, 1 and 5 μM). Data are represented as mean ± SD of three images.

Knowing that PFOA enters and accumulates in the cytosol of Caco-2 cells, we performed a series of assays to evaluate its metabolic and toxicological effects on the cells. Given that many metabolic pathways, such as glycolysis, occur in the cytosol [30], we began with the resazurin (alamarBlue) assay, a redox indicator that reflects cellular metabolic activity, and refined our subsequent assays based on the initial results. The cell metabolic activity was boosted by PFOA exposure, especially at low doses (+20 % at 1–10 μM) (Fig. 8A) but could not be related to ATP level (Fig. 8C). Moreover, no oxidative stress was detected except at 500 μM (Fig. 8D), which is undoubtedly an unrealistic exposure concentration. Unfortunately, no other studies on intestinal cells were available for comparison. In hepatic cells, one study showed that PFOA exerted a cytotoxic effect on the HepG2 cell line starting at 200 μM but did not induce an increase in ROS at concentrations tested between 5–400 μM [31]. Similarly, another study on neuronal cells exposed to PFOA for 24 h reported decreased cell viability and increased oxidative stress at concentrations above 250 μM, with ATP levels being affected from 400 μM onwards [32].

No membrane damage was detected by LDH assay (Fig. 8B) or SIMS imaging (Fig. 1). Interestingly, LDH release decreased at low doses, reaching a minimum at 0.5–1 μM (−10 %), before increasing and eventually plateauing at levels similar to the control. At low concentrations (0.1–5 μM), PFOA may inhibit LDH enzyme activities and

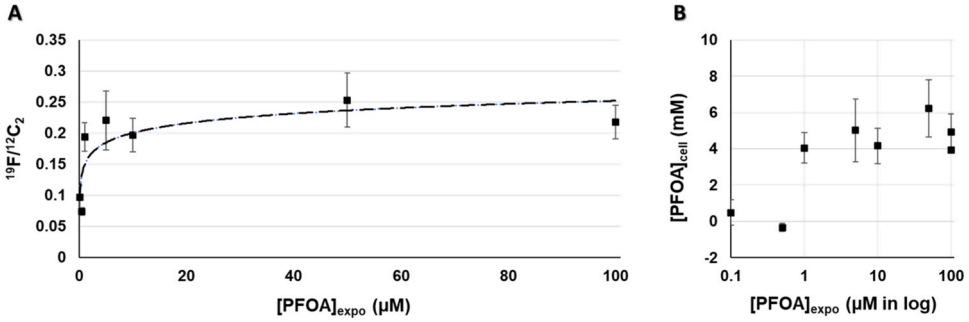

Fig. 4. Concentration of PFOA in the cytosol of Caco-2 cells by FIB-SEM-SIMS. (**A**) Ratio between $^{19}F^-$ and $^{12}C_2^-$ signal in function of the PFOA exposure concentration (μM). (**B**) Intracellular PFOA concentration (mM) in function of the PFOA exposure concentration (μM). The calibration curve used to estimate the PFOA intracellular concentrations was established as explained in the experimental section. Data are represented as mean ± SD of five images.

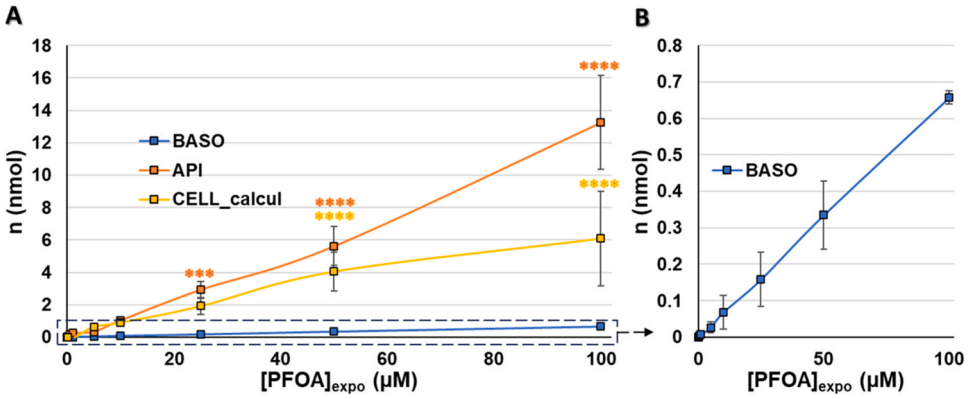

Fig. 6. PFOA quantification in the cell media: apical (API, orange, **A**) and basolateral (BASO, blue, **B**) media. Based on the initial quantity of PFOA and on the measured quantity in the API and BASO media after exposure, the quantity inside the cells was estimated (yellow). This quantity does not take into account the potential interactions of PFOA with the well/insert and may therefore be over-estimated. Data are represented as mean ± SD of three individual experiments. *P*-values (P) were calculated using two-way ANOVA. * P ≤ 0.05; * * P ≤ 0.01; * ** P ≤ 0.001; * *** * P ≤ 0.0001 vs. the control group.

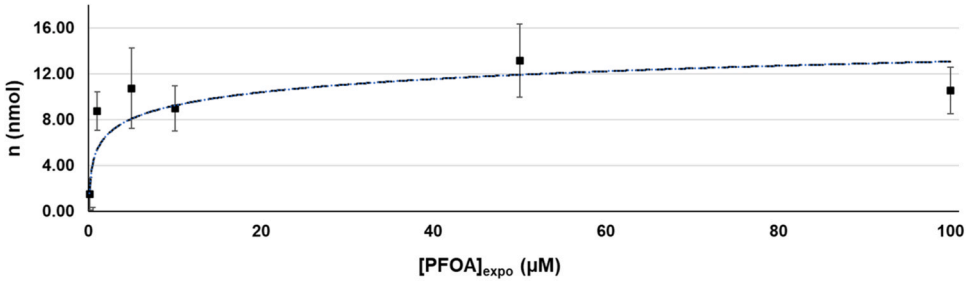

Fig. 7. Quantity of PFOA in the Caco-2 cell monolayer (deduced from Fig. 4 and Eq. 1).

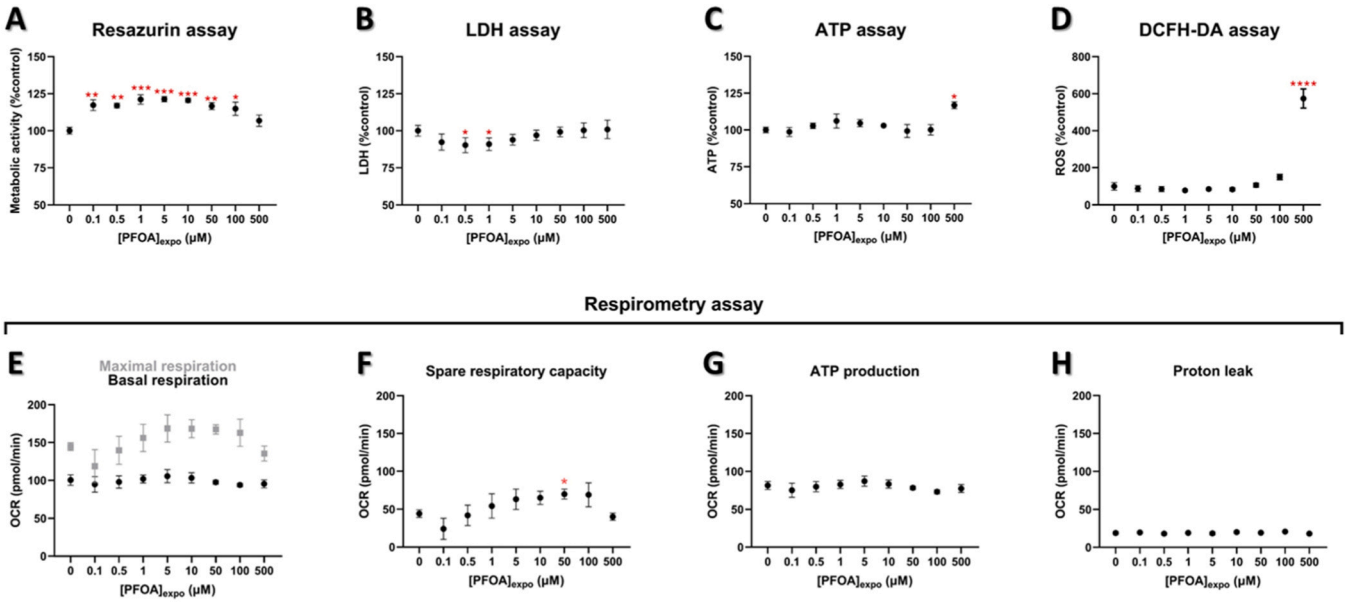

Fig. 8. Cell toxicity assays. (**A**) Resazurin assay (**B**) LDH assay (**C**) ATP assay (**D**) DCFH-DA assay (**E-H**) Respirometry assay: (**E**) Basal and maximal respiration (**F**) Spare respiratory capacity (**G**) ATP production (**H**) Proton leak. Data are represented as mean ± SEM of three individual experiments. *P*-values (P) were calculated using one-way ANOVA. * P ≤ 0.05; * * P ≤ 0.01; * ** P ≤ 0.001; * *** * P ≤ 0.0001 vs. the control group.

potentially other mechanisms linked to lactate metabolism as demonstrated by Obiako et al. [32]. This inhibition could explain the observed increase in cellular metabolic activity, as the metabolic pathway typically associated with lactate production might be redirected towards acetyl CoA synthesis, which induces NADH production. Resazurin, used in our assay, can be reduced to resorufin by NADH and other biologically abundant reductive species in the presence of mitochondrial or cytoplasmic reductases [33]. As PFOA concentration increases beyond a certain threshold, LDH release also increases, eventually reaching a plateau similar to the control. This increase may reflect slight cellular

damage or membrane disruption at higher PFOA concentrations, leading to the leakage of LDH into the extracellular space. Given the increase in cell metabolic activity that could not be correlated with ATP production and ROS generation, as well as the decrease in LDH activity at low concentrations, we performed a deeper analysis of the impact on mitochondrial metabolism using mitochondrial respirometry.

Minimal effects on mitochondrial respiration were observed (Fig. 8E-H). Only the maximal respiration and the spare capacity changed according to PFOA exposure concentration. For both parameters, the OCR decreased at the lowest dose (0.1 μM), then increased for higher doses until reaching a plateau. This decrease suggests that PFOA impacted mitochondria activity, but the cells counteracted this effect at higher concentrations, suggesting an adaptation to meet additional energy demands in case of another putative stress condition. The impact on mitochondrial activity could be related to the synthesis of mitochondria substrate, mitochondrial biogenesis (ATP production) or the uncoupling of the electron transfer chain [34]. However, regardless of the PFOA concentration, no impact on ATP production, proton leak, or basal respiration was observed. Therefore, when considering the results of our previous toxicity assays, the decrease in maximal respiration may be explained by a reduction in mitochondrial substrates in the cell, such as pyruvate, due to LDH inhibition. Consequently, the increase observed in the resazurin assay might be linked to this loss of pyruvate, indicating a metabolic induction to compensate. Moreover, another study demonstrated that there was no effect on isolated mitochondria from rat liver exposed to 100 μM PFOA, supporting the hypothesis of induced cellular dysfunction, such as LDH inhibition [35].

Even though cell toxicity assays investigated here did not show a clear toxic effect of PFOA, mass spectrometry analysis clearly demonstrated an uptake of PFOA by the intestinal cells and a high accumulation inside the cytosol, until reaching a concentration much higher than the nominal exposure concentration. While intracellular PFOA concentrations reached a plateau between 1–100 μM (Fig. 4), effects on cellular toxicity markers such as resazurin, ATP, LDH, DCFH-DA, and mitochondrial respiration markers varied across different exposure concentrations (Fig. 8). This divergence could be attributed to several factors. For instance, results from the resazurin and LDH assays clearly show a hormetic response. Previous studies have documented hormetic responses where low doses of toxins such as PFOA can induce beneficial effects or adaptive responses in cells, while higher doses may be detrimental. It is important to note that a single toxic chemical at a single dose can cause multiple endpoint damage. Thus, one effect might show a hormetic positive response, while another effect might show a negative response. Additionally, stimulation may simply be an indicator or precursor of an adverse effect. The toxicology community remains uncertain whether stimulation is beneficial or harmful. For PFAS, this hormesis has been observed in ecotoxicology studies [36] and epidemiological studies [37,38]. In those studies, doses usually refer to the PFOA exposure concentration (or blood concentration) without knowing the actual intracellular PFOA concentration. In our study, we take this a step further by demonstrating that the toxic effects at the cellular level are not linearly correlated to the intracellular PFOA concentration. To the best of our knowledge, there is no current published study showing the toxic effects of PFOA on Caco-2 cells for comparison. Moreover, in other in vitro toxicity studies on PFOA involving different cell types, this hormetic effect has not been observed. In addition to this hormetic effect, cellular responses to toxin exposure such as PFOA are multifaceted and may involve intricate signaling pathways and adaptive mechanisms that respond differently to varying concentrations of the chemical.

Further research on the effects of PFOA could be performed, such as proteomic or lipidomic analysis of the cytosol. Indeed, we have previously developed a methodology assessing the lipidomic impact of PFOA considering an in vivo mouse model [29], and this workflow could also be adapted to any other human cell model. Conversely, the high-resolution PFOA imaging and quantification approach developed in this current study could complement our previous in vivo study by providing more detailed information.

This complementary multi-technique approach, combining mass spectrometry analysis with widely used toxicology assays, has provided insightful information about the toxicity, intestinal absorption, and intracellular fate and concentration of PFOA in human intestinal Caco-2 cells after 24-h acute exposure, and paves the way for further toxicology research on PFAS both in vitro and in vivo.

4. Materials and methods

4.1. Chemicals

Chemicals, solvents and kit assays were purchased from the following sources: Dulbecco's modified eagle medium (DMEM) (Gibco, Belgium), DMEM-Glutamax (Gibco, Belgium), non-essential amino acids (NEAA) (Invitrogen, Belgium), penicillin/streptomycin (Pen/Strep) (Gibco, Belgium), heat-inactivated fetal bovine serum (FBS) (Invitrogen, Belgium), Dulbecco's modified phosphate buffered saline (DPBS) (Gibco, Belgium), trypsin-EDTA (Gibco, Belgium), dimethylsulfoxide (DMSO) (Sigma-Aldrich, Belgium), perfluorooctanoic acid (PFOA) (Sigma-Aldrich, Belgium), $^{13}C_8$-PFOA (Campro Scientific, Germany), ethanol (EtOH) (VWR, Belgium), alamarBlue™ Cell Viability Reagent (ThermoFischer Scientific, Belgium), CytoTox-ONE™ Homogeneous Membrane Integrity Assay (Promega, The Netherlands), CellTiter-Glo® 2.0 Cell Viability Assay (Promega, The Netherlands), CM-H2DCFDA General Oxidative Stress Indicator (ThermoFischer Scientific, Belgium), Seahorse XF Cell Mito Stress Test Kit (Agilent, Belgium), CyQUANT™ Cell Proliferation Assay (ThermoFischer Scientific, Belgium), glutaraldehyde (GA) (Sigma-Aldrich, Belgium), osmium tetroxide (OsO_4) (Sigma-Aldrich, Belgium), and Spurr resin (Polysciences, Germany).

4.2. Cell culture

The human colon cancer Caco-2 cell line was obtained from the American Type Culture Collection (ATCC® HTB-37™, USA). Caco-2 cells were cultured in DMEM-Glutamax supplemented with 10 % v/v FBS, 1 % v/v NEAA, and 1 % v/v Pen/Strep (called medium thereafter) and maintained at 37 °C in a 5 % CO_2 humidified atmosphere. The correct identity of the Caco-2 cell line was confirmed through the Human STR profiling cell authentication service provided by ATCC.

Until the needed number of cells is reached, cells were cultured in T75 flask. The medium was replaced every second day and the cell morphology was checked by light microscopy. Cells were trypsinized at 80–90 % confluency approximately twice a week, counted (using a Scepter 2.0 automated cell counter) and seeded into new T75 flasks at the appropriate seeding density.

4.3. Cell toxicity assays

4.3.1. Cell seeding

Caco-2 cells were seeded in 96-well plates at a concentration of 1×10^5 cells/mL in 200 μL medium and kept at 37 °C in a 5 % CO_2 humidified incubator for 21 days to ensure their complete cell differentiation. Meanwhile, the medium was renewed every 2–3 days, and cell morphology was checked using light microscopy.

4.3.2. Cell exposure

After the 21 days of differentiation, the medium was discarded and 200 μL/well of new medium containing increasing concentrations of PFOA (stock solution prepared in sterile water) from 0 to 500 μM were added (serially diluted in medium). Cells were maintained for 24 h at 37 °C in a humidified atmosphere of 5 % CO_2.

4.3.3. Cell metabolic activity (Resazurin assay, alamarBlue™)

The cell metabolic activity was evaluated by the resazurin assay. Resazurin is a cell-permeable and non-fluorescent compound, which is converted to fluorescent resorufin by metabolically active cells. After 24-h exposure, the medium containing PFOA was discarded and replaced with 200 μL/well of 400 μM resazurin in medium. After incubation for 1 h at 37 °C in a 5 % CO_2 humidified incubator in the dark, the fluorescence at 530-nm excitation and 590-nm emission wavelengths was measured with a fluorescence microplate reader (Spark 20 M, Tecan, Belgium). The reported values are expressed as a percentage of the negative control (unexposed cells).

4.3.4. Cell metabolic activity (ATP assay, CellTiter-Glo®)

The cell metabolic activity was also evaluated by the ATP assay, quantifying adenosine triphosphate (ATP) in the cells. The ATP is the energy source for all living cells and participates in many important biochemical reactions. After 24-h exposure, the plates were equilibrated at room temperature for 30 min 100 μL/well of CellTiter-Glo® Reagent were added in each plate and plates were mixed for 2 min on an orbital shaker to induce cell lysis. After 10-min incubation at room temperature, the luminescence was recorded using a microplate reader (Spark 20 M, Tecan, Belgium). The reported values are expressed as a percentage of the negative control (unexposed cells).

4.3.5. Cell membrane integrity (LDH assay, CytoTox-ONE™)

The cell membrane integrity was evaluated by the release of lactate dehydrogenase (LDH). LDH is a cytosolic enzyme, which is released into the cell culture medium in case the plasma membrane is damaged. After 24-h exposure, 100 μL/well of the exposure medium were transferred in another plate and incubated with 100 μL LDH-substrate. After 10 min, 50 μL of the stop solution was added. For the positive control (maximum LDH release), cells were previously lysed using Triton X-100. The fluorescence was measured at an excitation wavelength of 530 nm and an emission wavelength of 590 nm (Spark 20 M, Tecan, Belgium). The reported values are expressed as a percentage of negative control (unexposed cells).

4.3.6. Intracellular reactive oxygen species (DCFH-DA assay, CM-H2DCFDA molecular probes)

The level of reactive oxygen species (ROS) after PFOA exposure was evaluated by the DCFH-DA assay. DCFH-DA is a cell-permeable and non-fluorescent probe, which is deacetylated by intracellular esterases into non-fluorescent DCFH. In the presence of ROS, DCFH is oxidized to highly fluorescent DCF. Here, we use a derivative of fluorescein with a thiol-reactive chloromethyl group (chloromethyl-H_2DCFHDA), which allows for covalent binding to intracellular components, permitting even longer retention within the cell. The dye-loading concentration and loading time were optimized beforehand. After 21 days of differentiation and before cell exposure, the medium was discarded and replaced by 200 μL/well of 10 μM DCFH-DA diluted in PBS. After incubation for 1 h at 37 °C in a 5 % CO_2 humidified incubator in the dark, the dye was removed, and the cells were washed twice with PBS. Then, cells were exposed to PFOA as described above. After 24-h exposure, the fluorescence was measured at an excitation wavelength of 480 nm and an emission wavelength of 530 nm (Spark 20 M, Tecan, Belgium). Each plate contained 0.01 % H_2O_2 as a positive control. The reported values are expressed as a percentage of the negative control (unexposed cells).

4.3.7. Cell oxygen consumption rate (Seahorse assay)

The Seahorse XF cell mitochondrial stress test provides a complete mitochondrial profile, revealing important information not revealed by basal metabolic measurements alone. Seahorse XF Analyzers measure oxygen consumption rate (OCR) of living cells in a multi-well plate. The concentration of dissolved oxygen in an extremely small volume (2 μL) of medium is measured every few seconds above the monolayer of cells within the microplate. An integrated drug delivery system allows to sequentially inject up to four compounds per well of various types, including inhibitors, stimulators or substrates at defined intervals. The day before the assay, the three XFe96 sensor cartridges were filled with 200 μL/well of Seahorse XF calibrant and placed at 37 °C in a non-CO_2 incubator overnight. The seahorse assay media were prepared as follows: DMEM (without glucose) containing 2 mM of L-Glutamine, 2 mM of pyruvate and 10 mM of glucose. After 24-h exposure, the medium containing PFOA was discarded, the cells were washed once with the seahorse assay media and 175 μL/well of the seahorse assay media was added. The plates were incubated for 1 h at 37 °C in a 5 % CO_2 humidified incubator. Meanwhile, the cartridges were loaded with drugs as follows: 5 μM oligomycin, 1 μM FCCP, 2.5 μM antimycin, and 1.25 μM rotenone, and placed in the seahorse instrument for calibration. Then, the microplate of the cartridge was replaced by the plate containing the cells. After analysis, the remaining assay medium was removed, and the plates were stored at −80 °C upon further cell proliferation assay (for normalization).

4.3.8. Cell proliferation (CyQUANT® assay)

The CyQUANT cell proliferation assay enables to determine the density of cells in culture. The dye exhibits a strong fluorescence enhancement when binding to cellular nucleic acids. The plates were equilibrated at room temperature. Then, 200 μL/well of the dye 400-fold diluted in the 1X cell-lysis buffer were added in the plates that were incubated for 5 min at room temperature in the dark. The fluorescence was measured at an excitation wavelength of 480 nm and an emission wavelength of 520 nm (Spark 20 M, Tecan, Belgium). As seahorse plates are not compatible with microplate reader, lyzed cells were transferred to a new 96-well plate before measuring fluorescence.

4.4. PFOA localization and quantification inside the cells

4.4.1. Cell seeding

Caco-2 cells were seeded on uncoated Millicell® hanging cell culture inserts for 24-well plates (1-μm pore size; PET membranes, Sigma-Aldrich, Belgium) and cultured in 200 μL apical and 400 μL basal media (same medium as described above). For 21 days (until reaching complete cell differentiation), apical and basal media were renewed every 2–3 days, and cell morphology was checked using light microscopy.

4.4.2. Cell exposure

At the day of exposure, basal medium was renewed and PFOA solution (stock solution diluted in sterile water) from 0 to 100 μM concentration range was added at the apical side. Cells were maintained for 24 h at 37 °C in a humidified atmosphere of 5 % CO_2. The isotopic enrichment was performed by exposure of the Caco-2 cells to $^{13}C_8$-PFOA (the eight carbons of the PFOA molecule are labelled ^{13}C). The isotopic $^{13}C/^{12}C$ ratio provided information on local PFOA enrichment for low-concentration exposure without third-party contamination (e.g., fluorine from the Spurr resin). The stock solution of 50 μg/mL was diluted in 100 % methanol, and thus a maximum concentration of 5 μM PFOA (< 5 % methanol) was used to avoid any toxicity to the cells.

4.4.3. Sample preparation for imaging

Cells in insert were fixed with 5 % v/v glutaraldehyde in DPBS for 12 h at 4 °C, then post-fixed with 1 % v/v osmium tetroxide in Milli-Q® water for 1 h at room temperature. Cells were dehydrated in a series of graded ethanol solutions (0 %, 30 %, 50 %, 70 %, 90 %, and 100 %) for 10 min each (and 2 h for the 100 % solution). The PET membrane covered by the cells was detached from the cell culture inserts using a scalpel, deposited in a mold, and embedded in Spurr resin. The resin was polymerized in the oven at 60 °C for 48 h and then, air cured for a few days. The resin blocks were sliced into 300-nm semi-thin sections using an ultramicrotome (Leica, Austria) and the sections were deposited on silicon wafers (Siltronix, France). The quality of the sections was

checked using light microscopy.

4.4.4. FIB-SEM-SIMS analysis

The images were acquired with a Focused Ion Beam - Scanning Electron Microscope (Scios DualBeam, ThermoFisher, The Netherlands) coupled to a Secondary Ion Mass Spectrometer (LIST, Luxembourg) (FIB-SEM-SIMS). After loading the samples into the chamber and before the analysis, a plasma cleaning of the chamber and the samples was performed (2 cycles, 30 min/cycle, 5 min break), contributing to the removal of surface contamination [39]. The SIMS images were acquired with a 30 keV Ga^+ ion beam with a current of 100 pA. Images were recorded on a 256 × 256-pixel grid with a recording time of 4 ms/pixel (~4 min per ROI) and a field-of-view of 40 × 40 μm^2 (150 nm/pixel). Negative secondary ion mode was used for the detection of $^{19}F^-$, $^{12}C_2^-$ and $^{12}C^{14}N^-$. After SIMS acquisition, the same areas were imaged with a back-scattered electron (BSE) detector using the electron beam (5 keV, 0.2 nA). Images were recorded as a matrix of 6144 × 4096 pixels with a counting time of 5 µs/pixel. The SIMS and BSE data were processed with the ImageJ software (National Institute of Health, US). Images were presented in RGB color mode with the fluorine $^{19}F^-$ in red, the $^{12}C^{14}N^-$ in green and the BSE signal in gray scale. Specific regions of interest (ROIs) were identified, and signal intensity was extracted from these areas. For intracellular PFOA quantification, a four-point linear calibration curve was prepared with resin mixed with PFOA at concentrations ranging from 100 µM to 10 mM and analyzed using the same parameters as for imaging the cell samples. Further details can be found the supplementary materials.

4.4.5. NanoSIMS analysis

The Caco-2 cells exposed to $^{13}C_8$-PFOA were imaged with a NanoSIMS-50L instrument (Cameca, Gennevilliers, France). A 2 pA Cs^+ beam with a primary ion acceleration voltage of 8 keV and a sample bias of – 8 keV (impact energy of 16 keV) were used. Under these conditions, a spatial resolution of 150 nm is estimated. Instrument was tuned for a mass resolution M/ΔM > 5 000 and the simultaneous detection of the negative emitted ions $^{12}C^-$, $^{13}C^-$, $^{19}F^-$, and $^{12}C^{14}N^-$, as well as $^{32}S^-$, $^{35}Cl^-$, $^{31}P^{16}O_2^-$ (but not presented here). Each region of interest (ROI) was scanned 10 times employing a 256 × 256-pixel raster over a 35 × 35 μm^2 area, with a dwell time of 30 ms per pixel per slice (total acquisition time of ~ 5 h per ROI). After a drift correction, the 10 slices were summed with the ImageJ plugin OpenMIMS software (MIMS, Harvard University; www.nrims.harvard.edu) and processed by a median filter with three-pixel radius. Hue Saturation Images (HSI) were used to present the isotope $^{13}C/^{12}C$ ratio images. The rainbow scale ranges from blue, set to natural ratio (1.1 %, expressed as natural ratio), to red, where the ratio is several times above natural ratio (e.g., 1.3 % corresponds to an enrichment of 18.2 % above the natural ratio). Further details can be found the supplementary materials.

4.5. PFOA quantification in the cell media

4.5.1. Sample preparation

The 200 µL apical and 400 µL basolateral media from the cell imaging experiments were transferred in Eppendorf tubes and kept at −20 °C for further analysis. Prior to analysis, the media were equilibrated at room temperature, diluted to fit the calibration curve, and prepared with an internal standard. No extraction was performed on the media samples; they were analyzed directly without further treatment.

4.5.2. LC-MS/MS analysis

Sample analysis was carried out using a High-Performance Liquid Chromatography system (1290 Infinity II, Agilent) coupled to a High-Resolution Mass Spectrometer instrument (x500R QTOF, Sciex). The analytical column was a Zorbax Eclipse Plus C18 Rapid Resolution HT (2.1 ×50 mm^2, 1.8 µm particle size, Agilent) and the mobile phase consisted of an aqueous solution of ammonium acetate (2.5 mM) as eluent A and LC-MS grade acetonitrile as eluent B. Elution gradient was as follows: 0–1 min 30 % B, 8 min 95 % B, 11 min 95 % B, 12.5 min 30 %, 15 min 30 % B. The flow rate was fixed at 0.3 mL/min, the injection volume was 5 µL, and column temperature was 30 °C. The mass spectrometer was equipped with an Electrospray Ionisation (ESI) source operating in the negative mode.

PFOA was quantified by high-resolution multiple reaction monitoring (MRM^{HR}) using the most abundant precursor/product ion transitions (412.97 Da → 168.9890 Da) whereas the second most abundant transition (412.97 Da → 218.9860 Da) was used as qualifier. Retention time, parent and fragment masses were compared with reference standards to identify PFOA. A nine-point linear calibration curve was prepared with external standards, with concentrations ranging from 2 to 500 nM. Dilutions were performed if concentrations were above the highest standard. Quality control standards were analyzed every ten samples to monitor any drift of the equipment. The mass accuracy was controlled every hour during the sequence to maintain a mass difference lower than 5 ppm. The matrix effects in the MS detection of PFOA in cell media were evaluated for each dilution factor applied to the samples, and correction factors were applied accordingly. Further details can be found in the supplementary materials.

5. Statistical analysis

All results are presented as mean ± standard deviation. Data were analyzed by one-way (or two-way) ANOVA using GraphPad Prism software (GraphPad Software Inc., San Diego, CA, USA). Differences between groups were considered statistically significant when the *p*-value (P) is * $P \leq 0.05$; * * $P \leq 0.01$; * ** $P \leq 0.001$; * ** * $P \leq 0.0001$. N is the number of biological replicates. P and N values are specified in the corresponding figure caption.

Environmental implications

Perfluorooctanoic acid (PFOA) is a persistent organic pollutant that accumulates in living organisms and ultimately bioaccumulate in the human body leading to major health issues. The bioaccumulation in the different organisms including the human body mainly occurred via ingestion. Using high spatial resolution mass spectrometry imaging, we were able to localize and quantify PFOA inside intestinal epithelial cells. The methodology developed, integrating in vitro assays and novel analytical techniques, is very useful to address concerns and questions regarding the fate and potential impacts of other perfluoroalkylated substances, a very topical subject, in any organisms, tissue and cell type.

CRediT authorship contribution statement

Maria A. Subirana: Investigation. **Dirk Schaumlöffel:** Writing – review & editing, Investigation. **Charlotte B. A. Stoffels:** Writing – original draft, Visualization, Validation, Methodology, Investigation, Formal analysis. **Jean-Nicolas Audinot:** Writing – review & editing, Supervision, Methodology, Funding acquisition, Conceptualization. **Sébastien Cambier:** Writing – review & editing, Supervision, Methodology, Formal analysis. **Arno C. Gutleb:** Writing – review & editing, Supervision. **Muriel Mercier-Bonin:** Writing – review & editing, Supervision, Methodology, Funding acquisition, Conceptualization. **Tom Wirtz:** Writing – review & editing, Supervision. **Cédric Guignard:** Writing – review & editing, Investigation. **Jens C. Schwamborn:** Writing – review & editing, Supervision. **Gemma Gommez:** Investigation, Formal analysis. **Denis Pittois:** Investigation.

Declaration of Competing Interest

The authors declare that they have no known competing financial interests or personal relationships that could have appeared to influence the work reported in this paper.

Acknowledgments

Funding: This work was co-funded by the Luxembourg National Research Fund via grant INTER/ANR/18/12545362.

Author contributions

JNA and MMB conceived the original idea and formulated the research goals. CBAS, SC, JNA and MMB designed the research methodology. SC, JNA, MMB, ACG, JCS, TW supervised the research study. CBAS, JNA, MASM and DS acquired the NanoSIMS images and treated the data. CBAS, CG and DP conducted the LC-MS/MS analysis and treated the data. CBAS and GG performed the Seahorse assay and treated the data. CBAS performed all other experiments, validated the results, and treated the data. CBAS, SC, JNA and MMB interpreted the results. CBAS wrote the manuscript. SC, JNA, MMB, ACG, JCS and TW revised and edited the manuscript. All authors discussed the conclusions and commented on the manuscript.

Appendix A. Supporting information

Supplementary data associated with this article can be found in the online version at doi:10.1016/j.jhazmat.2024.136205.

Data availability

Data will be made available on request.

References

[1] Evich, M.G., Davis, M.J.B., McCord, J.P., Acrey, B., Awkerman, J.A., Knappe, D.R. U., Lindstrom, A.B., Speth, T.F., Tebes-Stevens, C., Strynar, M.J., Wang, Z., Weber, E.J., Henderson, W.M., Washington, J.W., 1979. Per- and polyfluoroalkyl substances in the environment. Science (2022), 375. https://doi.org/10.1126/science.abg9065.

[2] Li, J., Wang, L., Zhang, X., Liu, P., Deji, Z., Xing, Y., Zhou, Y., Lin, X., Huang, Z., 2022. Per- and polyfluoroalkyl substances exposure and its influence on the intestinal barrier: an overview on the advances. Sci Total Environ 852, 158362. https://doi.org/10.1016/j.scitotenv.2022.158362.

[3] Lupton, S.J., Huwe, J.K., Smith, D.J., Dearfield, K.L., Johnston, J.J., 2012. Absorption and excretion of 14C-perfluorooctanoic acid (PFOA) in Angus cattle (Bos taurus). J Agric Food Chem 60, 1128–1134. https://doi.org/10.1016/j.scitotenv.2024.174071.

[4] Pérez, F., Nadal, M., Navarro-Ortega, A., Fàbrega, F., Domingo, J.L., Barceló, D., Farré, M., 2013. Accumulation of perfluoroalkyl substances in human tissues. Environ Int 59, 354–362. https://doi.org/10.1016/J.ENVINT.2013.06.004.

[5] Shi, L., Zheng, J., Yan, S., Li, Y., Wang, Y., Liu, X., Xiao, C., 2020. Exposure to perfluorooctanoic acid induces cognitive deficits via altering gut microbiota composition, impairing intestinal barrier integrity, and causing inflammation in gut and brain. J Agric Food Chem 68, 13916–13928. https://doi.org/10.1021/acs.jafc.0c05834.

[6] Wang, Y., Chang, W., Wang, L., Zhang, Y., Zhang, Y., Wang, M., Wang, Y., Li, P., 2019. A review of sources, multimedia distribution and health risks of novel fluorinated alternatives. Ecotoxicol Environ Saf 182, 109402. https://doi.org/10.1016/J.ECOENV.2019.109402.

[7] Steenland, K., Zhao, L., Winquist, A., Parks, C., 2013. Ulcerative colitis and perfluorooctanoic acid (PFOA) in a highly exposed population of community residents and workers in the Mid-Ohio Valley. Environ Health Perspect 121, 900. https://doi.org/10.1289/EHP.1206449.

[8] Rashid, F., Ahmad, S., Irudayaraj, J.M.K., 2020. Effect of perfluorooctanoic acid on the epigenetic and tight junction genes of the mouse intestine, 2020, Vol. 8, Page 64 Toxics 8, 64. https://doi.org/10.3390/TOXICS8030064.

[9] Zhang, L., Rimal, B., Nichols, R.G., Tian, Y., Smith, P.B., Hatzakis, E., Chang, S.C., Butenhoff, J.L., Peters, J.M., Patterson, A.D., 2020. Perfluorooctane sulfonate alters gut microbiota-host metabolic homeostasis in mice. Toxicology 431, 152365. https://doi.org/10.1016/J.TOX.2020.152365.

[10] Kleszczyński, K., Gardzielewski, P., Mulkiewicz, E., Stepnowski, P., Składanowski, A.C., 2007. Analysis of structure-cytotoxicity in vitro relationship (SAR) for perfluorinated carboxylic acids. Toxicol Vitr 21, 1206–1211. https://doi.org/10.1016/J.TIV.2007.04.020.

[11] Kleszczyński, K., Składanowski, A.C., 2011. Mechanism of cytotoxic action of perfluorinated acids. III. Disturbance in Ca2+ homeostasis. Toxicol Appl Pharm 251, 163–168. https://doi.org/10.1016/J.TAAP.2011.01.002.

[12] Miao, C., Ma, J., Zhang, Y., Chu, Y., Li, J., Kuai, R., Wang, S., Peng, H., 2015. Perfluorooctanoic acid enhances colorectal cancer DLD-1 cells invasiveness through activating NF-κB mediated matrix metalloproteinase-2/-9 expression. Int J Clin Exp Pathol 8, 10512.

[13] Kimura, O., Fujii, Y., Haraguchi, K., Kato, Y., Ohta, C., Koga, N., Endo, T., 2017. Uptake of perfluorooctanoic acid by Caco-2 cells: involvement of organic anion transporting polypeptides. Toxicol Lett 277, 18–23. https://doi.org/10.1016/j.toxlet.2017.05.012.

[14] Han, X., Kemper, R.A., Jepson, G.W., 2005. Subcellular distribution and protein binding of perfluorooctanoic acid in rat liver and kidney. Drug Chem Toxicol 28, 197–209. https://doi.org/10.1081/DCT-52547.

[15] K. Li, J. Liu, C.R.M. Grovenor, K.L. Moore, NanoSIMS Imaging and Analysis in Materials Science, Https://Doi.Org/10.1146/Annurev-Anchem-092019–032524 13 (2020) 273–292. https://doi.org/10.1146/ANNUREV-ANCHEM-092019–032524.

[16] Nuñez, J., Renslow, R., Cliff, J.B., Anderton, C.R., 2018. NanoSIMS for biological applications: current practices and analyses. Biointerphases 13, 3–301. https://doi.org/10.1116/1.4993628.

[17] De Castro, O., Audinot, J.N., Hoang, H.Q., Coulbary, C., Bouton, O., Barrahma, R., Ost, A., Stoffels, C., Jiao, C., Dutka, M., Geryk, M., Wirtz, T., 2022. Magnetic sector secondary ion mass spectrometry on FIB-SEM instruments for nanoscale chemical imaging. Anal Chem 94, 10754–10763. https://doi.org/10.1021/acs.analchem.2c01410.

[18] Audinot, J.N., Philipp, P., De Castro, O., Biesemeier, A., Hoang, Q.H., Wirtz, T., 2021. Highest resolution chemical imaging based on secondary ion mass spectrometry performed on the helium ion microscope. Rep Prog Phys 84. https://doi.org/10.1088/1361-6633/AC1E32.

[19] Hilgers, A.R., Conradi, R.A., Burton, P.S., 1990. Caco-2 cell monolayers as a model for drug transport across the intestinal mucosa. Pharm Res 7 902–910. https://doi.org/10.1023/A:1015937605100.

[20] Dykstra, M.J., Reuss, L.E., 2003. Biological Electron Microscopy: Theory, Techniques, and Troubleshooting. Springer, US.

[21] Tan, C.W., Gardiner, B.S., Hirokawa, Y., Layton, M.J., Smith, D.W., Burgess, A.W., 2012. Wnt signalling pathway parameters for mammalian cells. PLoS One 7, e31882. https://doi.org/10.1371/JOURNAL.PONE.0031882.

[22] Ghasemi, M., Turnbull, T., Sebastian, S., Kempson, I., 2021. The mtt assay: utility, limitations, pitfalls, and interpretation in bulk and single-cell analysis. Int J Mol Sci 22. https://doi.org/10.3390/ijms222312827.

[23] Quent, V.M.C., Loessner, D., Friis, T., Reichert, J.C., Hutmacher, D.W., 2010. Discrepancies between metabolic activity and DNA content as tool to assess cell proliferation in cancer research. J Cell Mol Med 14, 1003–1013. https://doi.org/10.1111/J.1582-4934.2010.01013.X.

[24] Lavogina, D., Lust, H., Tahk, M.J., Laasfeld, T., Vellama, H., Nasirova, N., Vardja, M., Eskla, K.L., Salumets, A., Rinken, A., Jaal, J., 2022. Revisiting the resazurin-based sensing of cellular viability: widening the application horizon. Biosensors 12. https://doi.org/10.3390/bios12040196.

[25] Urry, L.A., Cain, M.L., Wasserman, S.A., Minorsky, P.V., Reece, J.B., Campbell, N. A., 2017. Campbell biology. Pearson Education, Inc.,.

[26] ECHA, Support Document for Identification of Pentadecafluorooctanoic Acid (PFOA) as a substance of very high concern because of its CMR and PBT properties., (2013) 1–66.

[27] Luby-Phelps, K., 2000. Cytoarchitecture and physical properties of cytoplasm: volume, viscosity, diffusion, intracellular surface area. Int Rev Cytol 192, 189–221. https://doi.org/10.1016/S0074-7696(08)60527-6.

[28] Maso, L., Trande, M., Liberi, S., Moro, G., Daems, E., Linciano, S., Sobott, F., Covaceuszach, S., Cassetta, A., Fasolato, S., Moretto, L.M., De Wael, K., Cendron, L., Angelini, A., 2021. Unveiling the binding mode of perfluorooctanoic acid to human serum albumin. Protein Sci 30, 830. https://doi.org/10.1002/PRO.4036.

[29] Stoffels, C.B.A., Angerer, T.B., Robert, H., Poupin, N., Lakhal, L., Frache, G., Mercier-Bonin, M., Audinot, J.N., 2023. Lipidomic profiling of PFOA-exposed mouse liver by multi-modal mass spectrometry analysis. Anal Chem 95, 6568–6576. https://doi.org/10.1021/acs.analchem.2c05470.

[30] Chandel, N.S., 2021. Glycolysis. Cold Spring Harb Perspect Biol 13. https://doi.org/10.1101/CSHPERSPECT.A040535.

[31] Florentin, A., Deblonde, T., Diguio, N., Hautemaniere, A., Hartemann, P., 2011. Impacts of two perfluorinated compounds (PFOS and PFOA) on human hepatoma cells: cytotoxicity but no genotoxicity? Int J Hyg Environ Health 214, 493–499. https://doi.org/10.1016/J.IJHEH.2011.05.010.

[32] Obiako, P., Sevcik, A., Sayes, C.M., 2023. Rapid enzymatic activity model (REAM) to decipher the toxic action of per- and polyfluoroalkyl substances. Food Chem Toxicol 182, 114117. https://doi.org/10.1016/J.FCT.2023.114117.

[33] Rampersad, S.N., 2012. Multiple applications of Alamar Blue as an indicator of metabolic function and cellular health in cell viability bioassays. Sens (Basel) 12, 12347–12360. https://doi.org/10.3390/S120912347.

[34] Marchetti, P., Fovez, Q., Germain, N., Khamari, R., Kluza, J., 2020. Mitochondrial spare respiratory capacity: mechanisms, regulation, and significance in non-transformed and cancer cells. FASEB J 34, 13106–13124. https://doi.org/10.1096/FJ.202000767R.

[35] Starkov, A.A., Wallace, K.B., 2002. Structural determinants of fluorochemical-induced mitochondrial dysfunction. Toxicol Sci 66, 244–252. https://doi.org/10.1093/TOXSCI/66.2.244.

[36] Sun, T., Ji, C., Li, F., Wu, H., 2024. Time is ripe for targeting per- and polyfluoroalkyl substances-induced hormesis: global aquatic hotspots and implications for ecological risk assessment. Environ Sci Technol 58, 9314–9327. https://doi.org/10.1021/acs.est.4c00686.

[37] Lin, N., Zhang, Y., Su, S., Feng, Y., Wang, B., Li, Z., 2023. Exposure characteristics of legacy and novel per- and polyfluoroalkyl substances in blood and association

with hypertension among low-exposure population. J Hazard Mater 459, 132185. https://doi.org/10.1016/J.JHAZMAT.2023.132185.

[38] Tan, Y., Zeng, Z., Liang, H., Weng, X., Yao, H., Fu, Y., Li, Y., Chen, J., Wei, X., Jing, C., 2022. Association between perfluoroalkyl and polyfluoroalkyl substances and women's infertility, NHANES 2013–2016. Int J Environ Res Public Health 19. https://doi.org/10.3390/ijerph192215348.

[39] D. Fox, H. Zhang, Helium ion microscopy, 2018. https://doi.org/10.1007/978–981-13–0454-5_8.